Exploring the influence of a wave energy farm on the wave induced bottom friction on the Swedish west coast

Ola Kalén

Degree project for Bachelor of Science in

Earth Sciences

15 hec

Department of Earth Sciences

University of Gothenburg

2009 B-580

Abstract

Surface waves play an important role for the distribution of sediment in shallow basins. This paper explores how a reduction of the energy in the wave field due to a proposed farm of wave energy converters could influence the bottom sediment dynamics on a location close to Smögen on the Swedish west coast. A brief outline of the system of energy conversion to be used at the site is given. The decrease of the wave-induced bottom friction velocity, u*, is used to estimate the change in sediment transport at the seabed. Calculations are carried out for the location of the proposed site, as well as for shallower depths closer to the coastline, with the assumption of a constant flux of wave energy. These results are then compared to another set of calculations with a reduced level of wave energy flux, caused by the future wave energy farm. The rate of reduction of the flux used is 30 %, a somewhat tentative figure that is believed to be of realistic proportions. Computations are performed using an 8-year time series of wave data derived from the combined information from satellites, on site wave-buoy measurements and wind and wave models. The results show that the change in sediment dynamics due to the assumed level of reduction of wave energy flux, caused by the wave energy farm, may not be very significant at the proposed location outside of Smögen. This result is supported by a low decrease of the mean friction velocity, as well as the morphology of the coastline, which is rocky and with low rates of sediment transport.

Contents

1. Introduction 3
1.1 The Lysekil project 4
1.2 Wave energy farm Sotenäs 6
2. Theory 7
2.1 Linear wave theory 7
2.2 Energy considerations 10
2.3 Ocean wave spectrum 12
2.4 Energy absorption for point absorbers 14
2.5 Sediment transport and friction velocity 16
3. Wave data 19
4. Methods 19
5. Results 21
5.1 Verification of the results 21
5.2 Bottom friction velocity 22
6. Discussion and conclusions 24
6.1 Choices and limitations of parameters 24
6. 2 Friction velocity and sediment movement 25
7. Acknowledgments 26
8. References 26

1. Introduction

Surface waves in the ocean are a large contributing factor to the process of sediment distribution in shallow basins. The motions of surface waves may reach down to depths exceeding 200 meters (Harris and Coleman, 1998). Compared with the effects on the sediment transport induced by currents, wave action is often times of greater importance (Soulsby, 1997). A reduction of the energy levels in the wave field thus has the potential to alter the dynamics of the sediments at the seabed in areas of limited depth. A system for conversion of wave energy to electricity, named the Lysekil project, has been developed at Uppsala University. Various aspects of possible impacts on the marine environment by the installation of devices for energy conversion have been explored in connection with this project. These studies investigate effects caused by the presence of the physical structures in the ocean. Bio-fouling impacts and artificial reef effects have been studied by (Langhammer, et al., 2009). The possible change in flow patterns that the future installed devices could cause was modeled by (Persson, 2009). Since the devices absorb power from the waves they could possibly also influence the sediment transport. This is the approach of the present paper. The question if this influence would be significant is tested on a proposed wave energy farm outside of Smögen.

1.1 The Lysekil project

Wave power research with the aim of converting ocean wave energy to electricity has since 2002 been carried out by the division for Electricity within the Swedish Centre for Renewable Electric Energy Conversion at Uppsala University. A wave power concept called the Lysekil project has been developed and tested at a research site on the Swedish west coast (Leijon et al., 2008). The site is located 2 km south of Lysekil at 58,19° N, 11,36° E, shown in figure 1, and has a depth of approximately 25 m. The first wave energy converter (WEC) was launched in March 2006.

Figure 1. *The site for the offshore wave power plant. The red diamond and the red dot indicate the position of the WEC and the measurement station respectively.*

The WEC of the Lysekil project is a point absorber that consists of a direct driven linear generator, located on the seabed, with a cylindrical semi-submerged buoy at the surface that

absorbs the wave energy, as outlined in figure 2. A translator with magnets mounted between spacers, is connected to the buoy by a rope. To keep the rope under tension, springs are attached to the translator. End stop springs to handle mechanical overload are mounted at the top. The translator moves inside a stator consisting of a three phase winding. More details of the system technology are given in (Leijon et al., 2005).

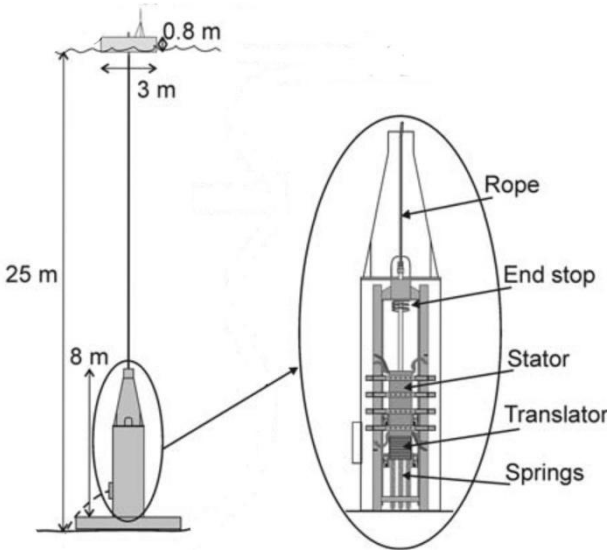

Figure 2. *Overview of the WEC (*Leijon et al, 2008, ©O.Danielsson).

When a wave crest elevates the buoy, the translator is pulled upwards. The kinetic energy in the translator is then induced as electricity in the stator and also stored as mechanical energy in the spring. The energy stored in the spring is induced in the stator as the spring pulls down the buoy in the succeeding wave trough. The rated power of the generator is 10 kW at a voltage of 200 V and translator speed of 0.67 m/s, giving a nominal current of 29 A. An example of the performance of the WEC is given in figure 3.

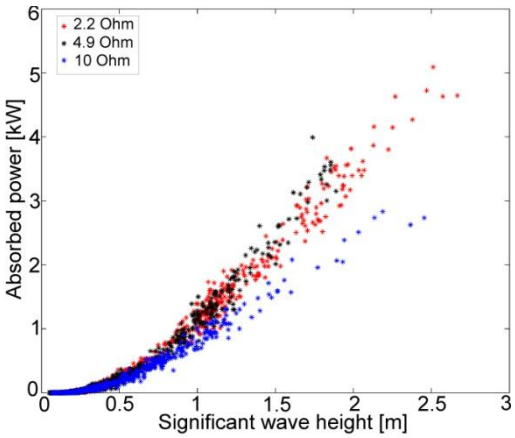

Figure 3. *Power absorption dependencies on resistive load (of the buoy, generator and sea cable configuration) and significant wave height during two months in the spring of 2006. Each sample represents a half hour average. (Engström et al., 2007).*

Other types of wave energy conversion systems use turbines or hydraulics to convert the energy. The wave motion is converted to a motion with higher speeds, more suitable for conventional generators. This results in relatively complex systems with several moving parts.

The advantage of the direct driven linear generator is its simpler mechanical system, requiring less maintenance. The complex transmission of the power to the grid, owing to the variability of the frequency of the generated voltage, is one drawback. For a thorough outline of contemporary systems, see (Cruz, 2008).

1.2 Wave energy farm Sotenäs

The Swedish company Seabased, with ties to the Swedish Centre for Renewable Electric Energy conversion at Uppsala University, is planning to construct a wave energy farm outside of Smögen on the Swedish west coast, location given in figure 4.

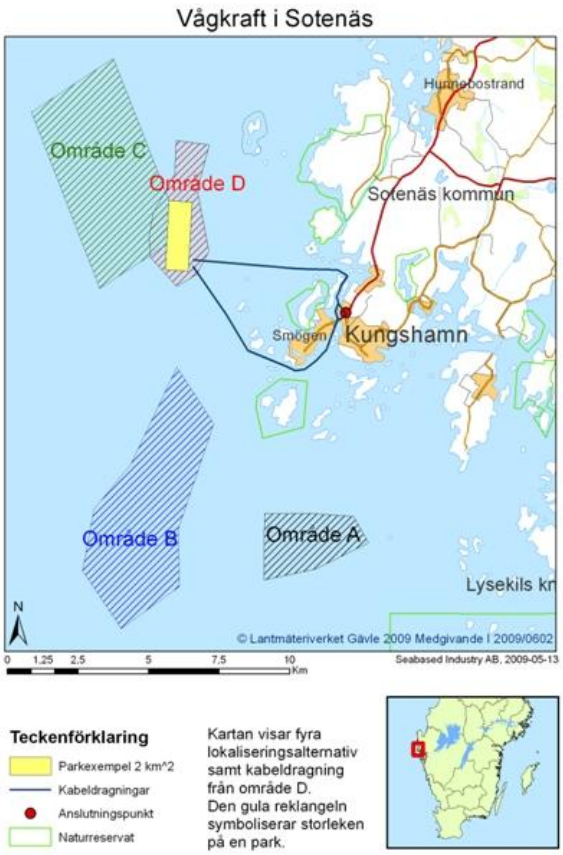

Figure 4. *Localization of the future wave energy farm. The yellow rectangle marks the location of the farm. (©Seabased Industry AB).*

Using the same technology as in the Lysekil project, the park is planned to consist of a maximum of 420 interconnected WECs with a total installed effect of 10 MW. The WECs will be placed in rows on an area the size of approximately 0.5 km^2. Farm outline and array configuration will be discussed further in chapter 2.4.

A marine geological survey of the area was carried out by Sveriges Geologiska Undersökning (SGU) (Nordgren and Lind, 2007). The location of the planned farm corresponds approximately to what is referred to as area C in this survey. The depth in area C ranged from 60 m in the western end to 50 m in the eastern end. The sediment type found in the major part of this area, shown in figure 5, was postglacial clay, consisting mainly of particles with grain size 0.2 to 2 µm.

In small zones, surrounding the bedrock, glacial clay as well as postglacial medium sand to gravel, with particles of grain size 0.5 to 60 mm, was encountered in layers above the glacial clay.

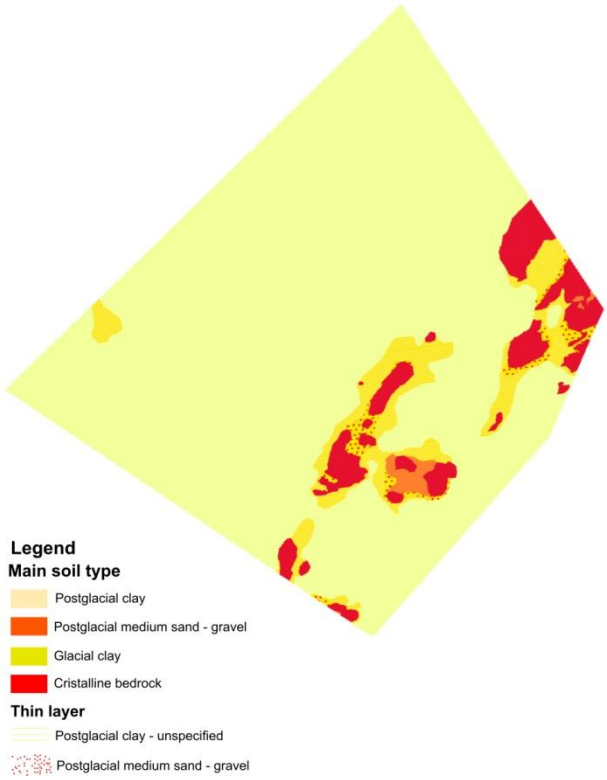

Figure 5. *Sediment distribution in the seabed within area C. (Nordgren and Lind, 2007).*

Sediment distribution can be classified as erosion, transport and accumulation seabeds. Erosion seabeds are suspect to continuous stress that prevents deposition of small grains. Accumulation seabeds represent the opposite with low activity, which favors deposition. Transport seabeds lend characteristics from both accumulation and erosion seabeds with infrequent resuspension events. The postglacial clay could be classified as an accumulation seabed, while the glacial clay is an erosion seabed. Apart from a mobile thin layer on top, they are not subject to much movement. The postglacial medium sand to gravel could be said to belong to the transport seabed type. It would be the type of sediment encountered in the area most sensitive to changes in levels of bottom stress.

2. Theory

2.1 Linear wave theory

The major part of ocean wave energy is created by wind, which in turn is caused by the circulation of solar energy in the atmosphere. Friction is generated between the wind and the surface of the ocean and this initiates the creation of surface waves. What begin as tiny ripples or capillary waves will in time develop to larger waves if the exposure to the wind continues. The disturbance of the surface, which is the wave, is influenced by gravity, which acts as a force to reestablish equilibrium. Waves grow over the whole basin in which they travel, which means

that the wave height is dependent on the distance to the nearest coast in the direction of the wind, called the fetch. The wave transports energy and continues to grow until the sea state reaches equilibrium, where the input of energy by the wind is balanced by wave breaking in the form of white caps. This state is called a fully developed sea. Very little of the energy is lost until the wave eventually reaches the coast where the energy dissipates when the wave breaks and the friction against the bottom increases.

Airy wave theory or linear wave theory can be used to describe the propagation of surface gravity waves in a homogenous fluid. The surface gravity wave is the type of wave that is relevant to the conversion of wave energy to electricity. Other types of ocean waves such as tidal waves and internal waves are not considered here.

The governing equations in the linear wave theory are the continuity equation:

$$\frac{\partial \rho}{\partial t} + \nabla(\rho \mathbb{u}) = 0 \tag{1}$$

and the Navier-Stokes equation

$$\frac{\partial \mathbb{u}}{\partial t} + \mathbb{u}(\nabla \mathbb{u}) = -\frac{1}{\rho}\nabla P + \mu \nabla^2 \mathbb{u} + \frac{1}{\rho}\mathbb{f} \tag{2}$$

where ρ is the density, $\mathbb{u}$ the velocity vector of a fluid element, P the pressure, $\mathbb{f}$ the external forces of the fluid element and μ the kinematic viscosity.

In order to simplify the problem and linearize the governing equations the following assumptions have to be made: Consider surface gravity waves of constant form and period T propagating in the x-direction in an ocean of uniform depth h. The wave-height H is small compared to the wavelength λ. It is further assumed that the fluid is incompressible, irrotational and that effects of turbulence, surface tension and viscosity can be neglected.

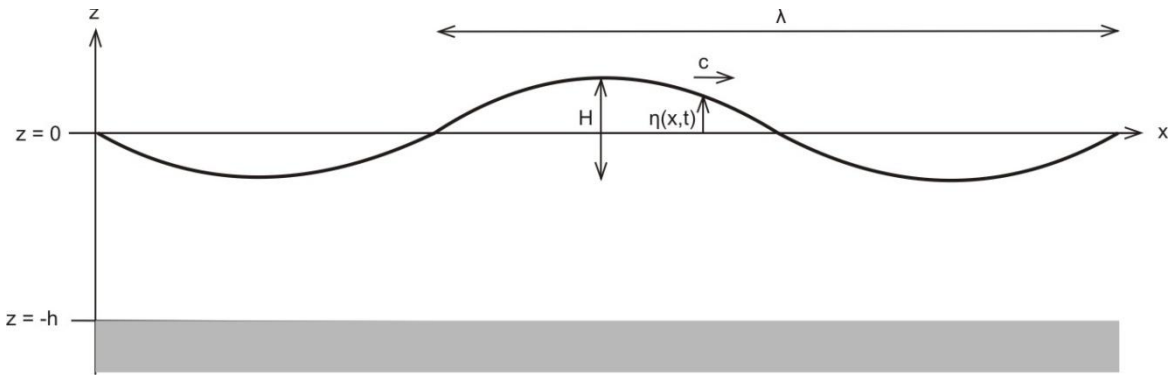

Figure 6. *Surface wave definitions.*

For an irrotational fluid, a velocity potential can be introduced such that

$$\mathbb{u} = \nabla \phi \tag{3}$$

which, if applied to the continuity equation, yields the Laplace equation:

$$\nabla^2\phi = 0 \tag{4}$$

Boundary conditions must be satisfied at the bottom and the free surface. The three linearized boundary conditions are (Kundu, 2008):

the kinematic bottom boundary condition

$$\left.\frac{\partial\phi}{\partial z}\right|_{z=-h} = 0 \tag{6}$$

the kinematic surface boundary condition

$$\frac{\partial\eta}{\partial t} = \left.\frac{\partial\phi}{\partial z}\right|_{z=0} \tag{7}$$

and the dynamic surface boundary condition

$$\left.\frac{\partial\phi}{\partial t}\right|_{z=0} = -g\eta \tag{8}$$

If the surface elevation is assumed to be of the form

$$\eta(x,t) = \frac{H}{2}\cos(kx - \omega t) \tag{9}$$

where k = 2π/λ is the wave number and ω = 2πf is the angular frequency, the solution to the Laplace equation (4) will be

$$\phi = \frac{H\omega}{2k}\frac{\cosh\ k(z+h)}{\sinh\ kh}\sin(kx - \omega t) \tag{10}$$

from which the velocity components for the fluid element are found as

$$u = \frac{H\omega}{2}\frac{\cosh\ k(z+h)}{\sinh\ kh}\cos(kx - \omega t) \tag{11}$$

$$w = \frac{H\omega}{2}\frac{\sinh\ k(z+h)}{\sinh\ kh}\sin(kx - \omega t) \tag{12}$$

Substitution of (9) and (10) into the boundary condition (8) yields the dispersion relation

$$\omega^2 = gk\ \tanh kh \tag{13}$$

The phase speed of the waveform, c = ω/k then gives

$$c = \sqrt{\frac{g}{k}\tanh kh} = \sqrt{\frac{g\lambda}{2\pi}\tanh\frac{2\pi h}{\lambda}} \tag{14}$$

which shows that the phase speed is dependent of the wavelength. Waves for which phase speed is a function of wavelength are called dispersive, because waves of different wavelengths propagate with different speeds and disperse i.e. separate from each other.

For deep water, where kh >>1, tanh kh tends to 1, the phase speed is approximated to

$$c = \sqrt{\frac{g}{k}} = \sqrt{\frac{g\lambda}{2\pi}} \tag{15}$$

The limit for which the deep-water approximation is valid is usually set to h ≥ λ/2. This is visualized by evaluating tanh(2πh/λ) at a depth of h = λ/2, whose value is approximately 0.996. A wave in the deep-water regime is the type of wave best suited for energy conversion, since no energy is lost to friction against the seabed.

Consider a group of dispersive waves propagating in the same direction with the same height, but with slightly different wavelengths. The speed of the individual waves will thus be different. It can be shown (Kundu, 2008), by superimposing the components of the different waves, that the energy of a wave does not travel with the phase speed, but with the speed of the whole wave packet, the group speed, which is equal to

$$c_g = \frac{d\omega}{dk} \tag{16}$$

which, by the derivation of the dispersion relation (13), is found to be

$$c_g = \frac{c}{2}\left(1 + \frac{2kh}{\sinh\ 2kh}\right) \tag{17}$$

Since sinh kh tends to infinity when kh >>1, the group speed for deep-water waves can be approximated to

$$c_g = \frac{c}{2} \tag{18}$$

2.2 Energy considerations

The energy content of surface gravity waves consists mainly of mechanical energy, normally measured in mean energy density per unit horizontal area. It is the sum of the potential energy due to the displacement of the water surface and the kinetic energy due to the motion of the fluid particles. In this context, the effects of surface tension and dissipation are negligible.

Integrating over the depth and averaging over a wavelength, the mean value of potential energy per unit area is

$$E_p = \overline{\int_{-h}^{\eta} \rho g z dz} - \int_{-h}^{o} \rho g z dz = \overline{\int_{0}^{\eta} \rho g z dz} = \frac{1}{2}\rho g \overline{\eta^2} = \frac{1}{16}\rho g H^2 \tag{19}$$

where the over bar denotes a mean value taken as either an average over one wavelength or a time average. The variance of the sea surface displacement is denoted by $\overline{\eta^2}$.

The mean kinetic energy per unit area is similarly found to be

$$E_k = \overline{\int_{-h}^{0} \frac{1}{2}\rho(u^2 + w^2)dz} \tag{20}$$

The integral is taken from the bottom to the mean water level, since the integral up to the surface would only introduce higher order terms. By using the fluid velocity components (11) and (12), the dispersion relation (13) and some trigonometric algebra, it can be found that

$$E_k = \overline{\int_{-h}^{0} \frac{1}{4}\rho \frac{gkH^2}{\sinh\ 2kh}[cos^2(kx - \omega t) + sinh^2 k(z + h)]dz} \tag{21}$$

which evaluates to

$$E_k = \frac{1}{2}\rho g\overline{\eta^2} = \frac{1}{16}\rho g H^2 \tag{22}$$

The total mean energy density per unit area is

$$E = E_p + E_k = \rho g\overline{\eta^2} = \frac{1}{8}\rho g H^2 \tag{23}$$

The transmission of energy due to wave motion is the pressure work done by the fluid. The mean energy flux per unit length of crest is the mean value of the energy that is transmitted through a vertical section, integrated over the whole depth:

$$\overline{J} = \overline{\int_{-h}^{o} pu\, dz} = \overline{\int_{-h}^{0} p'u\, dz} - \rho g\overline{u}\int_{-h}^{0} z\, dz = \overline{\int_{-h}^{o} p'u\, dz} \tag{24}$$

where the pressure p is expressed as a sum of a perturbation pressure p´ and a background pressure -ρgz. The linearized form of Bernoulli´s equation

$$\frac{\partial\phi}{\partial t} + \frac{P}{\rho} + gz = 0 \tag{25}$$

and the substitution of the velocity potential (10) then gives

$$p' = -\rho\frac{\partial\phi}{\partial t} = \frac{\rho H\omega^2}{2k}\frac{\cosh\ k(z+h)}{\sinh\ kh}\cos(kx - \omega t) \tag{26}$$

Substitution of (26) as well as the velocity component (11) into equation (24) then yields

$$\overline{J} = \overline{cos^2(kx - \omega t)}\frac{\rho H^2\omega^3}{4k\sin h^2 kh}\int_{-h}^{0} cosh^2 k(z + h)dz \tag{27}$$

which evaluates to

$$\bar{J} = \frac{1}{8}\rho g H^2 \left[\frac{c}{2}\left(1 + \frac{2kh}{\sinh\ 2kh}\right)\right] = E\ c_g \tag{28}$$

Equation (28) illustrates that the energy in surface waves propagates with the group speed. Using the deep-water approximation (18) to apply the relation $c_g = g/2\omega$, the energy flux is found to be

$$\bar{J} = \frac{1}{8}\rho g H^2 \frac{g}{2\omega} = \frac{\rho g^2 T H^2}{32\pi} \tag{29}$$

2.3 Ocean wave spectrum

The linear wave theory assumes that waves are harmonic sinusoids. A look at a real ocean, where the surface consists of many random waves of varying wavelength, period and direction, verifies that one sinusoidal wave is not enough to describe the surface of the ocean. The linearity of the theory means that a superposition of solutions is also a solution. A wave spectrum can be seen as a superposition of infinitely many linear waves with different wavelengths and directions. The spectrum specifies how the wave energy is distributed over these wavelengths and directions in the ocean. In this paper, however, only unidirectional spectra will be considered.

The background theory to wave spectra is the Fourier analysis, which proves that almost any function can be decomposed into an infinite series of harmonic sine and cosine functions. Consider a record of sea surface displacement $\eta(t)$, a continuous measurement recorded over the time period T. Using complex notation for the sine and cosine functions, $\eta(t)$ can be expressed as a Fourier series:

$$\eta(t) = \sum_{n=-\infty}^{\infty} \mathcal{Z}_n e^{2\pi i n f_0 t} \tag{30}$$

where

$$\mathcal{Z}_n = \frac{1}{T_0}\int_{-T_0/2}^{T_0/2} \eta(t) e^{-2\pi i n f_0 t} \tag{31}$$

frequency (Stewart, 2005). The Fourier transform converts the discrete time signal into a frequency domain. The spectrum, or spectral density S(f) of $\eta(t)$ can now be defined as

$$S(f) = \mathcal{Z}_n \mathcal{Z}_n{}^* \tag{32}$$

where $\mathcal{Z}_n{}^*$ is the complex conjugate of $\mathcal{Z}_n$. The integral of the spectrum S(f) of $\eta(t)$ is equal to the variance of the sea surface divided by 2π. Since the energy is proportional to this variance (23), S(f) is called energy or power spectrum. From this follows that the power in a certain sea is equal to the integral of the energy density, multiplied by the group velocity. An example of a spectrum is given in figure 7.

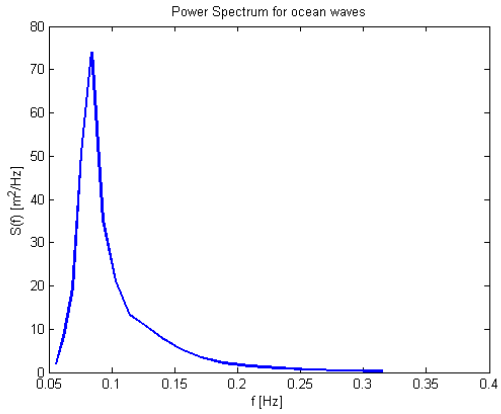

Figure 7. *Power spectrum modeled from wave data supplied by Fugro OCEANOR (details of the wave data are further explained in chapter 3).*

The spectral moments m_n are useful to calculate different characteristics of the spectrum. The nth moment of the frequency spectrum is given by

$$m_n = 2\pi \int_0^\infty f^n S(f) df = \int_0^\infty \omega^n S(\omega) d\omega \tag{33}$$

Different spectral parameters are used to characterize a sea state. The zeroth spectral moment, equal to the area under the spectrum curve or the variance of the sea surface is

$$m_0 = 2\pi \int_0^\infty S(f) df = \int_0^\infty S(\omega) d\omega = \overline{\eta^2} \tag{34}$$

By using (23) and (28), the mean energy flux can now be expressed as

$$\bar{J} = \rho g \int_0^\infty c_g(\omega) S(\omega) d\omega \tag{35}$$

The significant wave height is defined as the average height of the highest one third of the waves. The wave height is Rayleigh distributed and it can be shown that the significant wave height H_s is therefore related to the zeroth spectral moment as

$$H_s = H_{1/3} = H_{m0} = 4\sqrt{m_0} \tag{36}$$

The energy period T_e is calculated from

$$T_e = T_{m-10} = \frac{m_{-1}}{m_0} \tag{37}$$

The peak period T_p is the period corresponding to the peak of the wave spectrum.

Using that the energy density can be expressed as $\rho g m_0$, the wave energy flux for the deep-water approximation (28) can be given in terms of energy period and significant wave height as

$$\bar{J} = \frac{\rho g^2}{64\pi} T_e {H_s}^2 \tag{38}$$

If on site measurements of sea surface displacement are not available or are not dense enough to sufficiently define the energy spectrum, an idealized spectrum can be used to approximate the real ocean waves. Several such empirical spectra, with different limitations on fetch, topography and wind swell, exist. Examples are Pierson-Moskowitz, JONSWAP and DNV. One widely used spectrum is the two-parameter Bretschneider spectrum defined as (Lewandowski, 2004)

$$S(\omega) = \frac{1.25}{4}\frac{\omega_m^4}{\omega^5}H_s^2 exp\left[-1.25\left(\frac{\omega_m}{\omega}\right)^4\right] \tag{39}$$

where $\omega_m = 2\pi/T_e$ denotes the modal frequency.

2.4 Energy absorption for point absorbers

A wave energy converter can be classified as a point absorber, a terminator or an attenuator. Point absorbers are usually axisymmetric devices, which are small relative to the wavelength of the incident waves. Attenuators and terminators have finite dimensions compared to the incoming wave field and also have one dominant horizontal dimension. Terminators are positioned perpendicular to the incident waves, while attenuators are aligned with the direction of the waves, as shown in figure 8. An example of a system of the attenuator type is the Pelamis (Caracas, 2002).

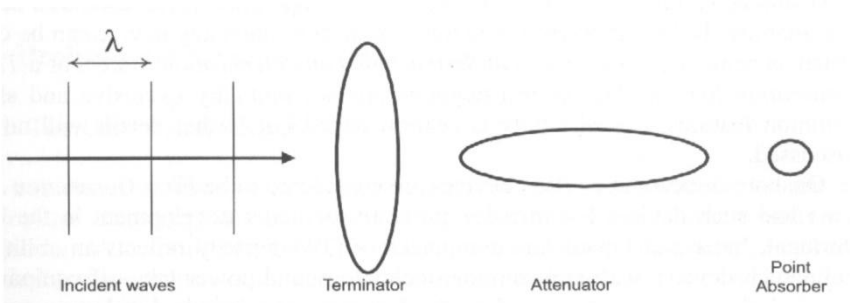

Figure 8. *Scale and orientation of a terminator, attenuator and point absorber (Cruz, 2008).*

The central concept of using a point absorber for wave energy conversion is to use a body with a damped oscillating motion that converts the energy of the wave to a load. The three dominating forces in the interaction between the wave and the body are diffraction, inertia and viscous forces. For a body that is large compared to the wavelength, diffraction forces dominate and the body will act as a wave breaker and a small amount of inertia is transferred to the body. If the body is much smaller than the wavelength, viscous or drag forces dominate, with a resulting energy loss to dissipation. These limits set the bound for the size of a point absorber, designed to maximize performance in a certain sea state (Engström, 2009). A system oscillating with a frequency close to that of the incident waves will achieve increased amplitude and speed and therefore transfer more energy from the buoy to the generator (Falnes, 2002). The damping

from the generator, geometry of the buoy and the inertia of the moving parts will all influence the performance. Tests have been made to optimize the amplitude response by adding inertia by the use of added mass (Engström et al., 2009).

The maximum theoretical power absorption for a point absorber has been given by (Falnes, 2002). Both the upper bound of the theoretical absorption of power P_{ub} , given as

$$P_{ub} = \frac{\pi \rho g}{4} \frac{V H_s}{T_e}$$

where V denotes the volume of the point absorber, as well as the incident power in the waves, limits the actual rate of absorption, as shown in figure 9. A maximum power capture ratio close to that of the dotted line has been achieved by the WECs of the Lysekil project (Engström et al., 2009).

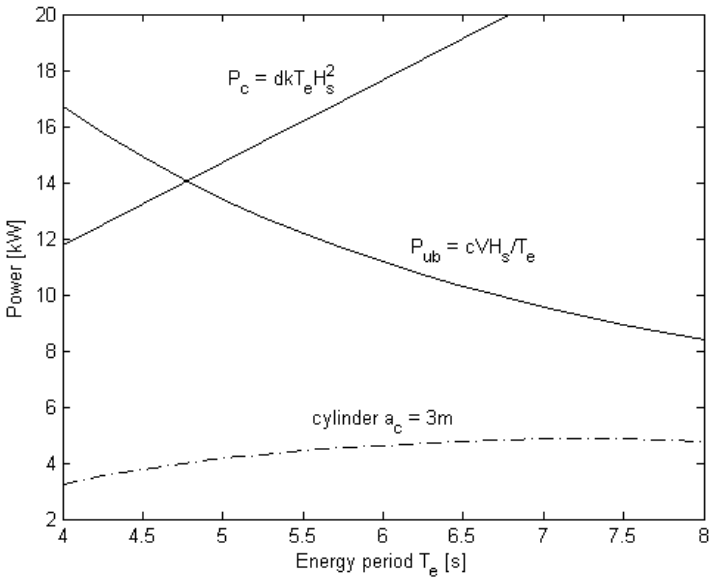

Figure 9. *Absorbed power for a semi-submerged cylinder with a radius d = a_c of 3 m. P_c denotes the available power in an ideal two dimensional case with $k = \rho g^2/64\pi$. Sea states are 17 time series based on a Bretschneider spectrum with constant H_s = 1 m. (Engström, 2009).*

According to (Waters, 2009), an energy period of around 6 s gives the highest annual amount of energy transport for site of the future wave energy farm, as proposed by Seabased. If this is applied to figure 9, the resulting ratio of absorbed power to available power is approximately 0.25 for a single point absorber.

How much power will then a whole wave energy farm absorb from the incoming waves? A wave power park will consist of an array of multiple point absorbers arranged in rows, an example of this is shown in figure 10.

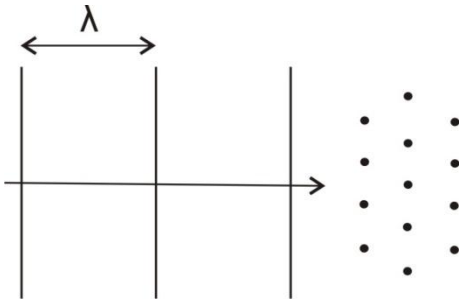

Figure 10. *Example of an array of multiple point absorbers.*

In contrast to a single point absorber, the absorption of an individual device in a row is now dependent of the direction of the incident waves. Each absorber removes power from the waves and thus there is less power left on the leeside of the absorber. This is also valid for entire rows of absorbers. The absorption of the first row results in less power available for the following row, as outlined in figure 11.

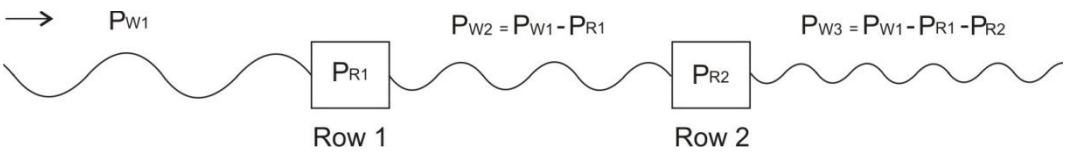

Figure 11. *Sketch of the absorption of power by consecutive rows of point absorbers. P_W denotes the available power in the wave field and P_R denotes the total power absorbed by an entire row of point absorbers.*

Theoretically it would be possible to install a large amount of rows and absorb all the power, but this would naturally not be economically justifiable. How much energy a cost-effective farm eventually will absorb is difficult to determine, owing to many factors. In this relatively new field of research much of the focus has been on improving the performance of the WECs, which might yet be far from optimized, and the problem of finding ideal outlines of whole farms is not very explored. As of today, there exists no commercially running wave energy farm, only a limited amount of practical experiments with single WECs has been run so far. The questions of array design and power capture are probed in (Ricci et al., 2007) and (Cruz et al., 2009). Judging from the findings in these papers, a capture rate of 30 % for a whole wave energy farm could be a realistic approximation.

2.5 Sediment transport and friction velocity

Out of the many factors influencing the distribution of sediments, grain size and bottom stress are important. The sorting of the sediments is to a large extent controlled by these parameters. Sediment samples can, as discussed in chapter 1.2, be used to describe the conditions at the seabed, but this approach is static and unsuitable to describe variations on shorter time scales.

An alternative is to focus instead on the bottom dynamics to better reflect kinematic conditions at the seabed. An outline of the processes of sediment transport is given in figure 12.

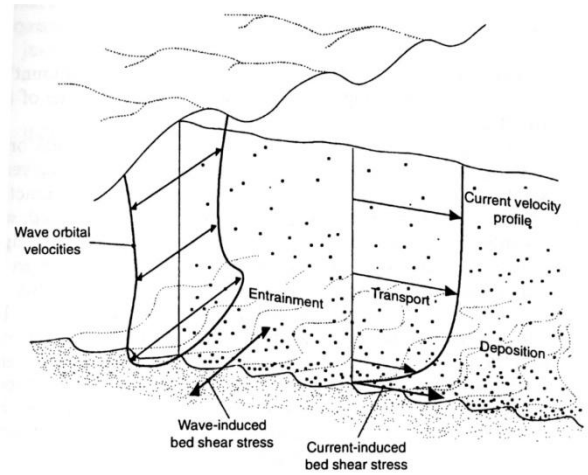

Figure 12. *Sediment transport processes (Soulsby, 1997).*

Waves and currents interact in all these processes that take place at the same time. Transportation is either suspended transport or bedload transport. If the velocities are high enough for a given grain size, the sediment will be put into suspension up to several meters over the bed. For a slower flow or larger grains, or a combination of both, the transport takes place by grains rolling and sliding along the bed, called bedload transport. When grains settle from suspension or come to rest in bedload transport, deposition occurs. Entrainment takes place due to the friction exerted on the seabed, leading to turbulent diffusion that may carry grains up into suspension.

Compared with currents, wave action is usually the major factor controlling sediment dynamics in shallow basins. The wave induced bottom boundary layer is orders of magnitude smaller than the current induced one which causes the stress levels associated with wave motion to be higher than those associated with currents of comparable magnitude (Soulsby, 1997; Nielsen 1992). In a study of the nutrient dynamics in southwest Kattegat, (Cristiansen et al., 1997) found that on a yearly basis, the wave induced shear stress was at least one order of magnitude higher than the current induced shear stress. It can also reach down to considerable depths; on continental shelves it has been modeled down to more 200 m with a resulting sediment movement (Harris and Coleman, 1998).

Effects induced by the waves and currents on the sediment dynamics occur mainly through the friction they exert on the seabed, the bed shear stress. The bottom friction velocity expresses shear stress in terms of velocity. It is a useful measure for the rate of dispersion and bedload sediment transport. It is defined as (Kundu, 2008)

$$u^* = \sqrt{\frac{\tau_0}{\rho}} \tag{40}$$

where τ_0 is the bottom shear stress. An estimate for the bottom stress due to waves is given by (Nielsen, 1992) as

$$\tau_0 = 0.5\rho f_w U_0^2 \tag{41}$$

where U_0 is the maximum orbital velocity above the bottom boundary layer and f_w is the wave friction factor. Now u^* can be expressed as

$$u^* = U_0\sqrt{0.5 f_w} \tag{42}$$

The orbital velocity U_0 at the bottom can be found from (11) (Dyer, 1986). For a spectrum of waves, a characteristic orbital velocity can be expressed as

$$U_0 = \frac{\pi H_s}{T_p \sin h\left(\frac{2\pi h}{\lambda_p}\right)} \tag{43}$$

where λ_p, the wavelength corresponding to the peak period T_p, is calculated from (13). Several empirical relations, based on grain size or flow regime, to calculate the wave friction factor exist. One Reynolds number relation (Nielsen, 1992), assuming a smooth bottom, is

$$f_w = \begin{cases} \frac{2}{\sqrt{Re}}, & Re \leq 3\ x\ 10^5 \\ 3.34\ x\ 10^{-3} + 1.05\ x\ \ 10^{-9} Re, & 3\ x\ 10^5 < Re < 1\ x\ 10^6 \\ 0.024 Re^{-0.123}, & 1\ x\ \ 10^6\ \leq Re \end{cases} \tag{44}$$

where the Reynolds number is calculated as

$$Re = \frac{U_0 H_s}{\upsilon 2 \sin h\left(\frac{2\pi h}{\lambda_p}\right)} \tag{45}$$

where ν denotes the kinematic viscosity.

Threshold velocity of grain movement is discussed in detail by (Dyer, 1986). It is defined as the minimum velocity required to move grains of a given diameter. For the regime of bottom dynamics at a given area to be changed, to transfer from a transport type sea bed ton an erosion type seabed for example, would require the velocity to exceed the given threshold values for long periods of times. Shown in figure 13 are threshold values in terms of friction velocity for varying grain sizes. It shows that a minimum friction velocity of 0.8 cm/s is required to dislodge sediment of grain size 0.01 mm, while the threshold value for the grain size 10 mm is approximately 10 cm/s.

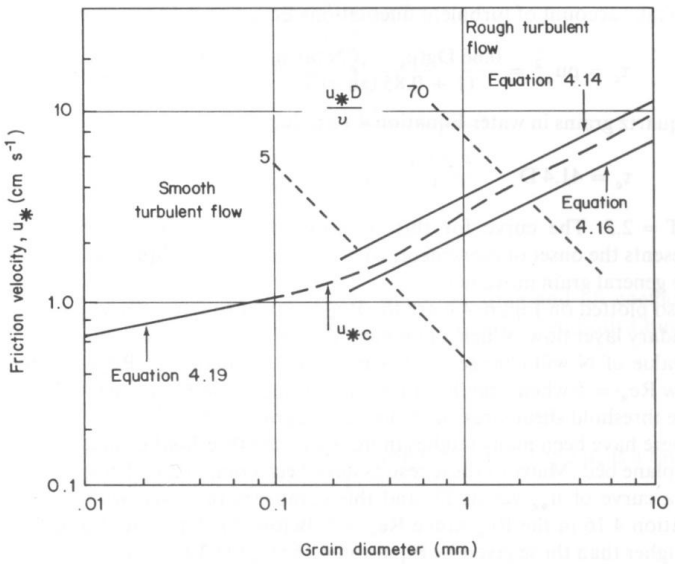

Figure 13. *Threshold friction velocity for grain movement. Equation 4.19, observations of White(1970). Dashed line, observations of Miller(1977). Equation 4.14 and 4.16 by Chepil(1958). Also shown by dashed lines 5 and 70 are the grain Reynolds numbers for smooth and rough turbulent flow. Image from (Dyer, 1986).*

3. Wave data

The wave data used in this thesis was purchased from Fugro OCEANOR of Norway to be used in the paper *Wave climate off the Swedish west coast* (Waters et al., 2009). Relevant wave parameters for every 6th hour, spanning over the years 1997-2004, are given. Each time step contains 18 different frequencies corresponding to spectral values. The data was computed by using the joint information from Satellites, wave-buoys and a wind and wave model, WAM (The WAMDI group, 1988) run by the European Centre for Medium range forecasts. The wave-buoy data originate from the location outside of Lysekil, described in section 1.2, and was sampled during the spring of 2005. This buoy was put up by The Swedish Centre for Renewable Electric Energy Conversion as a part of the Lysekil project. The satellite altimeter data was calibrated with the data from the buoy. The satellite data was, in turn, used to calibrate the WAM model.

Five of the thirteen studied points were located at depths of 15 to 30 m near shore. At these points the SWAN model (Simulating Waves Near shore, (Booij et al., 1999)) was used to adjust for the larger impact of the geography of the coastline and the seafloor. The wave-buoy data was also used to calibrate the SWAN model. The point used in the present paper is what is referred to as site 6 in (Waters et al,2009), located west of Smögen at 58,38° N, 11,00° E.

4. Methods

The aim was to investigate how a given outtake of energy by the wave energy farm would influence sediment transport at the bottom, proportional to a change of the friction velocity at the bottom. A change in the wave field will not only alter properties at the site of the change, but also inshore of the site. Therefore calculations, carried out by a routine in Matlab, were made for

the depth of the proposed site, 80 m, followed by calculations for 30, 20 and 10 m. This was done assuming that the mean energy flux is constant. For waves in the deep water regime, no energy is lost due to bottom friction. In each time step the quota h/λ > 1/2 is checked to find out if this is valid. The first step is to calculate the significant wave height H_s with spectral data according to (36). Since there are 18 frequencies given in the modeled wave data file, the integral of the spectrum (34) is approximated by

$$\sum_{k=1}^{18} S_k(\omega_k)\Delta\omega_k \tag{46}$$

Wavelengths for the given frequencies are then iterated with (13) as

$$\lambda_{k+1} = \frac{T^2}{2\pi}\tanh\left(\frac{2\pi h}{\lambda_k}\right) \quad (k = 1,2,\ldots) \tag{47}$$

Using these, the energy flux (35) is found with the use of the approximation (46). Next the peak period T_p is found by localizing the peak of the spectrum. With T_p known, the corresponding wavelength λ_p is computed as (47). Following this the orbital velocity (43), the Reynolds number (45), the wave friction factor (44) and finally the friction velocity (42) is calculated. When the depth h is changed, new wavelengths and spectra are calculated and the above process starts again. This whole routine is repeated once with the energy flux reduced by 30 %, simulating the impact of the wave energy farm. A flow chart for the computational steps is given in figure 14.

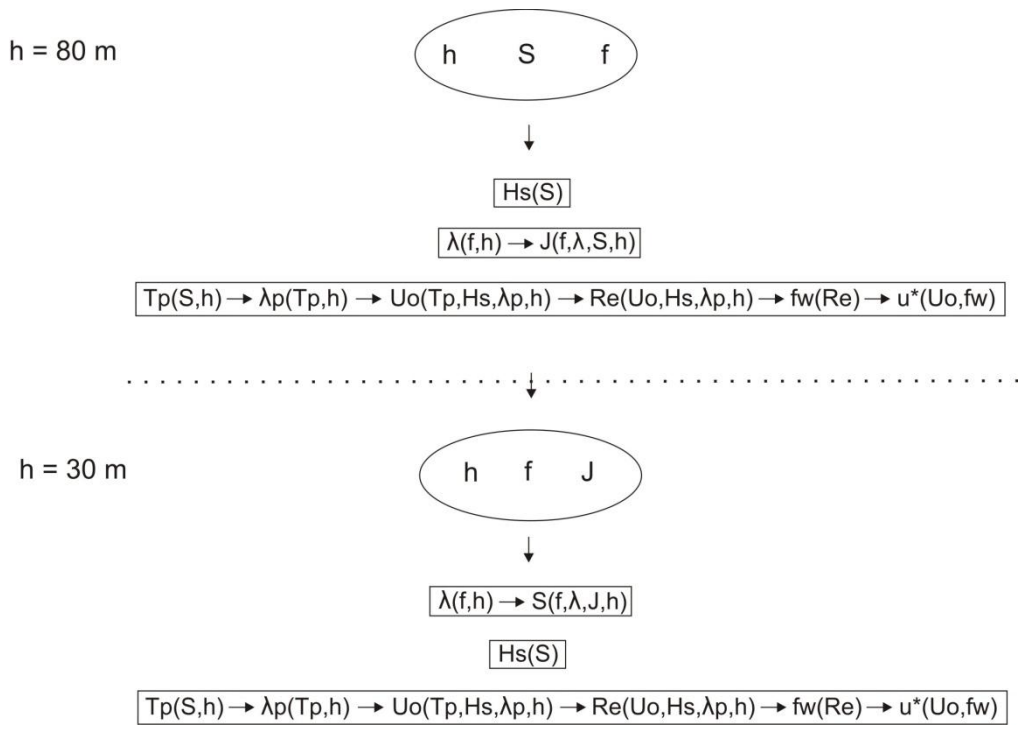

Figure 14. *Flow chart for the computations. Parameters in the ovals are given at each level, or as in the case of J, from the preceding level. Boxed parameters are computed using the entries given in the ovals and in the preceding boxes.*

5. Results

5.1 Verification of the results

To verify the output, comparisons were made to results in (Waters et al.,2009). In this study the energy flux was calculated with the deepwater approximation formula (39), using T_e and H_s as computed by Fugro OCEANOR, whereas the present paper uses the general case, finite depth formula (35), with H_s calculated using the 1-dimensional spectral data given in the wave data file. The results show good agreement, with the 8-year mean energy flux 5.1 kW/m, compared to 5.0 kW/m in (Waters et al.,2009).

Table 1. *Compared results are 8 year mean of energy flux with annual standard deviation, maximum energy flux and maximum significant wave height from 8 years of data.*

	J_{mean}±std [kW/m]	J_{max} [kW/m]	Hs_{max} [m]
Waters et al.	5.0±0.7	203.9	6.3
Present paper	5.1±0.8	218.9	6.3

The computed significant wave heights were compared to the wave heights in the wave data file. No significant differences were found here, as shown by the scatter plot in figure 15. The spectral values used to approximate the integral (34), which goes from zero to infinity, only cover a finite range of frequencies. A high-frequency tail can be added to the numerical spectrum to make up for this discrepancy, which was also done by Fugro OCEANOR. In this paper a rough estimate of the magnitude of the resulting additional energy flux by the addition of a high frequency tail was made. It was found to be of the order 0.05 kW/m, significantly less than the yearly standard deviation, and therefore not added in the computations.

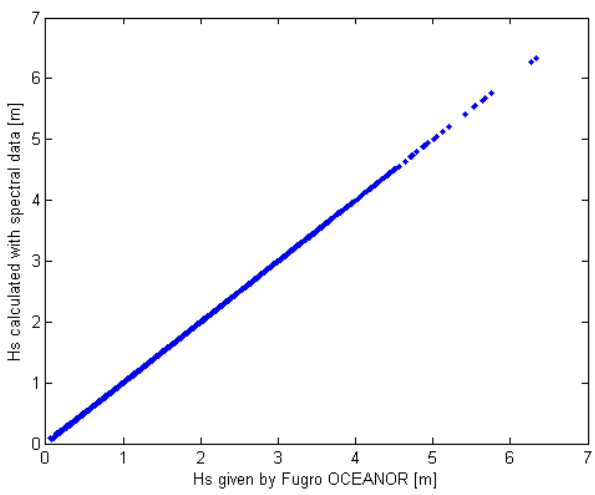

Figure 15. *Comparison between computed significant wave height and significant wave height given by Fugro OCEANOR.*

Further it was verified that the rate of decrease of H_s due to the loss of energy flux, caused by the wave energy park, was the same at all levels. This rate was found to be 16 %, which for the 80 m depth means that the mean H_s decreased from 1.04 m to 0.87 m.

5.2 Bottom friction velocity

In order to estimate how a decrease in the wave induced bottom friction velocity would influence the sediment transport, different statistics are presented. A significant change in the mean friction velocity could possibly lead to long term changes in the bottom sediment dynamics. Boxplots of the mean friction velocity for the two cases of energy flux are given for the depths 80, 30, 20 and 10 m in figure 16. The difference in magnitude and spread between the two cases is small at the first two depths. There is slightly more variation between the two shallowest depths, with the median at the 10 m depth decreasing from 1.7 to 1.5 cm/s.

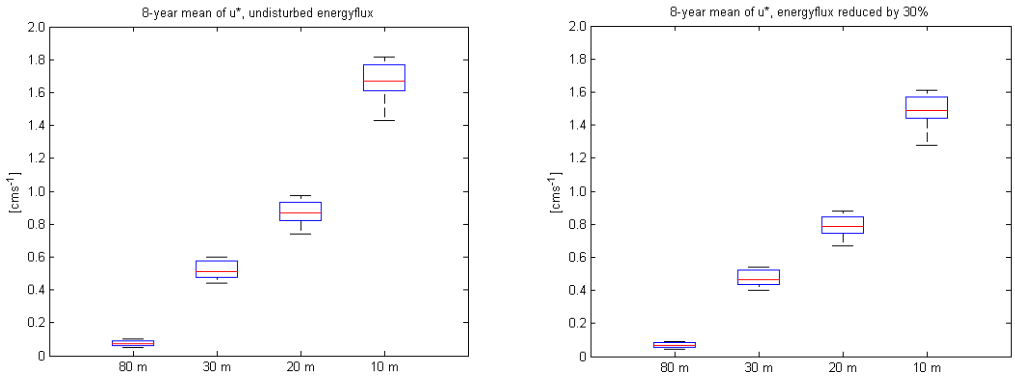

Figure 16. *Boxplots of 8 year mean of u* at 4 different depths, the left image with undisturbed energy flux and the right with a 30 % reduction. Each box contains 50 % of the data, limited below by the 25th percentile and above by the 75th percentile. The line through the box is the median. The ends of the lines extending from the boxes are the smallest and largest values, not further away than 1.5 boxlengths from the edge of the box.*

On a shorter timescale the highest values of friction velocity, which can initiate events of resuspension, are more important. Therefore a mean value of the highest 5 % of the values, denoted mean $u^*_{0.05max}$, is also shown in figure 13. The boxplots of figure 17 give that almost no changes due to the reduced flux occur at the 80 and 30 m levels. The decrease is most significant at 10 m where the median $u^*_{0.05max}$ goes from 5.5 to 4.5 cm/s. Thus the general trend for the two cases of energy flux for mean $u^*_{0.05max}$, with small differences at the two deeper levels and a slight increase of differences at the two shallower, is similar to that of mean u*.

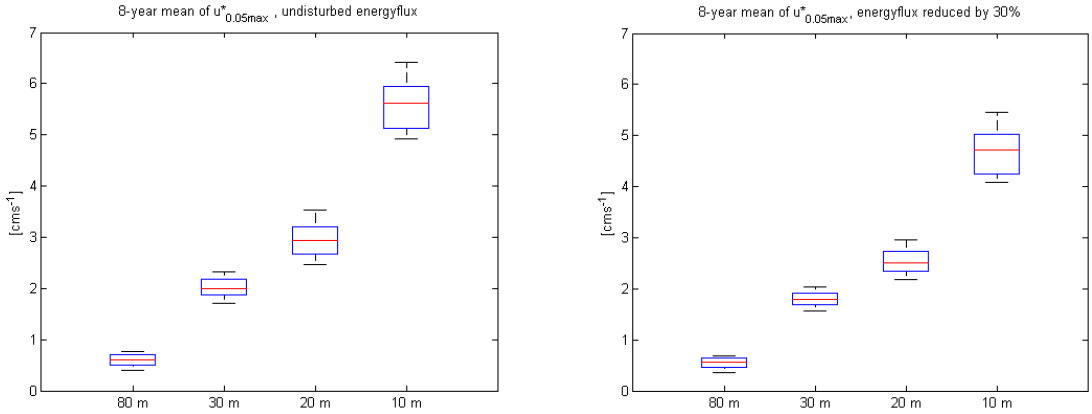

Figure 17. *Boxplots of 8 year mean of $u^*_{0.05max}$ at 4 different depths, the left image with undisturbed energy flux and the right with a 30 % reduction.*

The rates of change of mean u* and $u^*_{0.05max}$ due the reduction of the energy flux, caused by the wave energy farm, are summed in figure 18. A decrease of approximately 10 % is detected for both types of mean u* at the two deeper levels. The changes are more significant at the shallower levels of 20 and 10 m, with the highest entry, a decrease of $u^*_{0.05max}$ of approximately 16 %, at the 10 m depth.

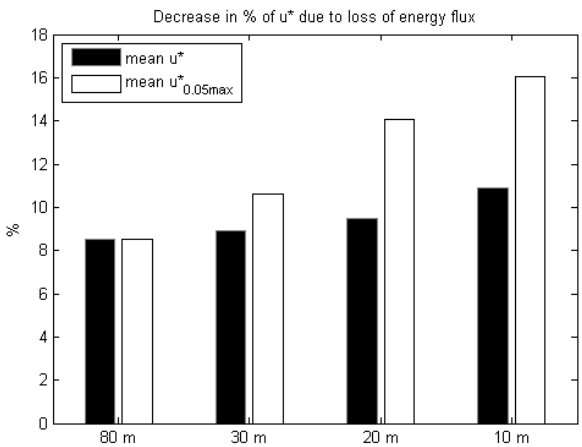

Figure 18. *Decrease of mean u* and mean $u^*_{0.05max}$ due to reduction of the energy flux.*

The threshold friction velocity for grain movement is a useful help for detecting a change in bottom dynamics. Different values of the threshold friction velocity, denoted $u^*_{critical}$, are used in figure 19 to display a ratio of the time during eight years that that the friction velocity exceeds the given threshold value.

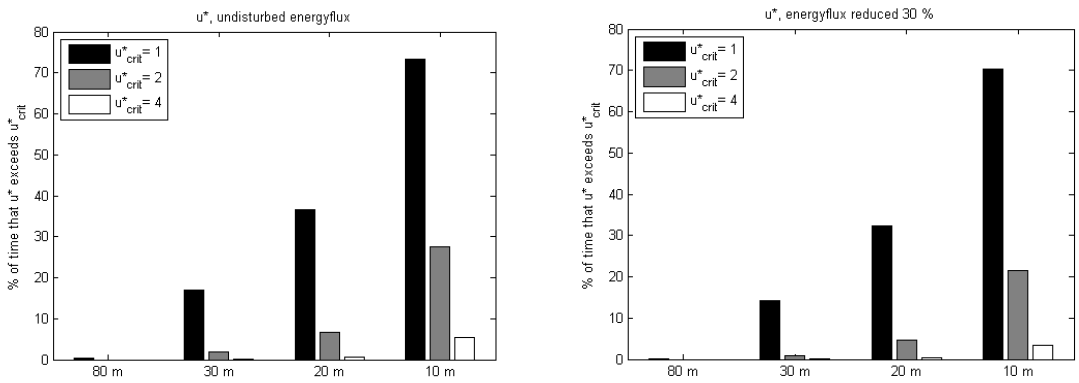

Figure 19. *Ratio of time during 8 years that u* exceeds 3 different threshold values* $u^*_{critical}$ *, given in cm/s in the legend. Left hand side shows values during the undisturbed energy flux and right hand side with the energy flux reduced by 30 %.*

Figure 19 shows that the changes in the ratio of the time during eight years that $u^*_{critical}$ is exceeded are small for all depths. Very little change is observed at the two deeper levels. The highest change in the time ratio is approximately 6 percentage units, occurring at 10 m for $u^*_{critical}$ = 2 cm/s, for which the time ratio decreases from 27 % to 21 %.

6. Discussion and conclusions

6.1 Choices and limitations of parameters

The values for $u^*_{critical}$ were chosen with the aid the discussions held in chapters 1.2 and 2.5. Figure 13 gives that a threshold velocity of approximately 2 cm/s is required to move the lower bound of the sediment postglacial medium sand to gravel. This is the sediment type encountered on the proposed site that is most prone to dislocation, as discussed in chapter 1.2.

The magnitude of the amount of energy that the wave energy farm absorbs will greatly influence the results. The rate of reduction of 30 % of the energy flux is motivated by the discussions carried out in chapter 2.4. As mentioned in this section, there are yet many uncertainties regarding this subject, but 30 % could be a realistic approximation as of today.

The relation for the wave friction factor (47) is based on a smooth bottom assumption. Figure 5 shows that the largest part of the seabed of the studied area consists of post-glacial clay, thus the smooth bottom assumption seems reasonable. According to (Jönsson, 2005) in a study of the Baltic Sea, the use of the smooth bottom assumption is justifiable for this area, with the errors limited to coarse bottoms, where the values of friction velocity are somewhat underestimated.

The results show that the influence of the reduction of the energy flux is higher at the locations closer to the shoreline. One limitation of this study is that it does not consider the impact on the actual coastline, but stops at a depth of 10 meters. Further sediment type data for the shallower depths would also enhance the conclusions.

6. 2 Friction velocity and sediment movement

With the limitations and assumptions discussed the results can now be interpreted. They show that the largest changes due to the assumed reduction of power by the wave energy farm occur on the depths of 20 m and 10 m. The decrease of mean $u^*_{0.05max}$ would be around 15 % while mean u* would decrease approximately 10 % at the two shallowest depths, according to figure 18. There is not much difference between the ratio of time that mean u* exceeds the threshold values, as shown in figure 19. The mean value of the friction velocity is probably more significant for longer lasting changes, as opposed to peak values that initiate resuspension events. Since the area studied is also one with a small rate of sediment transport, the small changes become even less important.

As a conclusion, the results suggest that the assumed reduction of the wave energy flux caused by the wave energy farm would not significantly alter the bottom sediment dynamics at the proposed site outside of Smögen. What supports this statement is, above all, the modeled low decrease of the mean bottom friction velocity. Peak values would decease slightly more, but are less probable to alter the long term conditions at the sea bed. The coastline at the proposed site is rocky with low rates of sediment transport, which greatly reduces the impact. A wave farm would be more probable to change sediment transport at a location where the shoreline consists mostly of sand as opposed to bedrock.

A further step for a future study could be to add on site turbulence measurements. These could then be compared to the calculated values for the friction velocity. The inclusion of current measurements might also be an improvement. Although believed to be of lesser importance than wave action, they could add to the total accuracy of a study. An effect not included in this paper is the change of direction of the incoming waves due to diffraction, caused by the wave energy farm. The arrays of wave energy converters will diffract the wave field, change its directions, and the distribution of the energy would then be altered. It could lead to either focusing or dispersion of the energy, depending on the surrounding topography and depth. Exploring these effects would enhance a future investigation. The impact of a reduced energy flux might also be more significant on a location with more energetic seas and a larger rate of sediment transport, such as the west coast of Denmark. A small reduction in the vast amounts of sediment that is transported along this coast could possibly have large effects on the morphology of the coastline.

7. Acknowledgments

Lars Arneborg, my supervisor, thank you for taking your time to answer my many questions, both the hard and the easy ones. You pointed me at an escape route when I thought I had reached a dead end. Thank you Jens Engström, my associate supervisor, for sharing your knowledge of a very exciting subject, the research of wave energy conversion. Fredrik Klingberg of SGU is thanked for very valuable input on the marine geology section. Lennart Bornmalm is acknowledged for connecting me with information regarding marine geology, Jan Sundberg of Seabased for supplying information about the Sotenäs wave energy park, Stephen Barstow and Gunnar Mörk of Fugro OCEANOR for discussions on wave data.

8. References

Bernhoff H, Sjöstedt E, Leijon M (2006) Wave energy resources in sheltered sea areas: A case study of the Baltic Sea, *Renewable Energy* 31, pp. 2164–2170.

Booij N, Ris R C, Holthuijsen L H (1999) A third-generation wave model for coastal regions. 1. Model description and validation, *Journal of geophysical research, vol 104, pp 7649-7666.*

Caracas M C (2003) The OPD Pelamis WEC: Current status and onward programme, *International Journal of Ambient Energy*, vol. 24, 2003.

Christiansen C, Gertz F, Lamia M J C, Lund-Hansen L C, Vang T, Jürgensen C (1997) Nutrient (P,N) dynamics in the southwestern Kattegat, Scandinavia: sedimentation and resuspension effects, *Environmental Geology 29 (1/2), pp 66-77.*

Cruz J (2008) Ocean Wave Energy, Springer, Berlin Heidelberg.

Cruz J, Sykes R, Siddorn P, Eatock Taylor R (2009) Wave Farm Design: Preliminary Studies on the Influences of Wave Climate, Array Layout and Farm Control, *Proceedings of the 8th European Wave and Tidal Energy Conference,* Uppsala, Sweden.

Dean R G, Dalrymple R A (1991) Water Wave Mechanics for Scientists and Engineers, Advanced Series on Ocean Engineering-vol. 2, World Scientific, Singapore.

Dyer K R (1986) Coastal and Estuarine Sediment Dynamics, Wiley, Chichester .

Engström J (2009) Hydrodynamic Modeling of the Energy Conversion from Ocean Waves to Electricity, Licentiate Thesis, Uppsala University, Sweden.

Engström J, Eriksson M, Isberg J, Leijon M (2009) A Wave Energy Converter with enhanced amplitude response at frequencies coinciding with Swedish west coast sea states by use of supplementary added mass, *Journal of Applied Physics 106.*

Engström J, Waters R, Stålberg M, Strömstedt E, Eriksson M, Isberg J, Henfridsson U, Bergman K, Asmussen J, Leijon M (2007) Offshore experiments on a direct-driven Wave Energy Converter, *Proceedings of the 7th European Wave and tidal Energy conference,* Porto, Portugal.

Falnes J (2002) Ocean waves and oscillating systems, linear interaction including wave-energy extraction, Cambridge University press, Cambridge.

Harris P T, Coleman R (1998) Estimating global shelf sediment mobility, *Marine Geology 150, pp 170-177.*

Isberg J, Eriksson M, Leijon M (2008) Transport of energy in polychromatic fluid gravity waves, *Journal of Engineering Mathematics 64, pp 15-23*

Jönsson A, Danielsson Å, Rahm L (2005) Bottom type distribution based on wave friction velocity in the Baltic Sea, *Continental Shelf Research 25, pp 419-435.*

Jönsson A, Broman B, Rahm L (2002) Variations in the Baltic Sea wave fields, *Ocean Engineering* 30, pp. 107–126.

Kundu P K, Cohen I M (2008) Fluid Mechanics, Academic Press Inc., San Diego.

Langhammer O, Wilhelmson D, Engström J (2009) Atrificial reef effect and fouling impacts on offshore wave power foundations and buoys – a pilot study, *Estuarine, Coastal and shelf Science, February 2009.*

Leijon M, Boström C, Danielsson O, Gustafsson S, Haikonen K, Langhamer O, Strömstedt E, Stålberg M, Sundberg J, Svensson O, Tyrberg S, Waters R (2008) Wave Energy from the North Sea: Experiences from the Lysekil Research Site, *Surveys in Geophysics, volume 29, pp 221–240*

Lewandowski E M (2002) The Dynamics of Marine Craft: Manouvering and Seakeeping. Advanced Series on Ocean Engineering-vol. 22, World Scientific, Singapore.

Nielsen P (1992) Coastal bottom boundary layers and sediment transport. Advanced Series on Ocean Engineering-vol. 4, World Scientific, Singapore.

Persson O (2009) Possible impact on hydrography and sediment transport by wave power park – numerical modeling, Master Thesis, Uppsala University, Sweden

Ricci P, Saulnier J B, Falcão A F de O (2007) Point-absorber arrays: a configuration study off the Portuguese West-Coast, *Proceedings of the 7th European Wave and tidal Energy conference,* Porto, Portugal.

Soulsby R (1997) Dynamics of marine sands, Tomas Telford Publications, London.

Stewart R H (2005) Introduction to Physical Oceanography, Texas A&M University.

Svendsen I, Jonsson I (1982) Hydrodynamics of Coastal Regions, Stougaard/Jensen, Copenhagen.

The WAMDI Group (1988) The WAM Model—a third generation wave prediction model, *Journal of Physical Oceanography* 18, pp. 1775–1810.

Waters R, Engström J, Isberg J, Leijon M (2009) Wave climate off the Swedish west coast, *Renewable Energy 34, pp. 1600-1606*